Indian Journal of Chemical Technology
Vol. 32, September 2025, pp. 650-663
DOI: 10.56042/ijct.v32i5.12941

Cycas inermis plant leaves extract as an environmental-friendly corrosion inhibitor extracted by efficient Soxhlet extraction technique for soft cast steel in 1 MH_2SO_4

Manohar R Rathod*[1], Vijaylaxmi T Talawar[2] & S K Rajappa[1]

[1]Department of Chemistry, Karnatak Science College, Dharwad, Karnataka-580 001, India
[2]P.G. Department of Mathematics, Karnatak Science College, Dharwad, Karnataka-580 001, India

*E-mail: manoharrathod125@gmail.com

Received 2 August 2024; accepted 11 August 2025

Plant extracts as corrosion inhibitors have received significant attention due to their potential activities and cost-effectiveness. In this current work, it is intended to utilize the inhibitive activity of the Cycas inermis plant leaves extract *(CILE)* to mitigate the corrosion of soft cast steel (SCS) in sulfuric acid medium and reduce the environmental risk. The studies revealed that the inhibition efficiency of *CILE* increases with higher concentrations of the inhibitor but decreases with rising temperatures. The maximum inhibition efficiency of 96.15% has been achieved at a concentration of 2.0 g/L. The adsorption of *CILE* on the SCS surface follows the Langmuir adsorption isotherm model. Surface morphology analyses of both uninhibited and inhibited SCS have been evaluated using scanning electron microscopy (SEM), atomic force microscopy (AFM), and water contact angle (WCA) measurements. SEM analysis indicated that the metal surface is significantly protected from aggressive corrosion due to the inhibitor. AFM visualization confirms the formation of a protective layer on the steel surface, which resulted in a reduction in surface roughness. Overall, this study demonstrates the potential of *CILE* as an effective, environmentally friendly corrosion inhibitor for soft cast steel in acidic environments.

Keywords: Corrosion current, Corrosion inhibitor, Cycas inermis, Soft cast steel, Soxhlet extraction technique

Introduction

Soft cast steel has been universally employed in numerous manufacturing factories since long ago, which including shipbuilding, civil engineering, automobiles, and home appliances[1]. Aqueous acids are frequently utilized in industrial operations for cleaning, pickling, and descaling, particularly in acidification procedures and oilfields[2,3]. These acidic solutions severely corrode metal surfaces, resulting in significant financial losses for numerous sectors. Consequently, it is critical to stop and combat rusting, and it appears, in our opinion, that changing the solution's condition could protect the material from corrosion. Because of their affordability, effectiveness, and ease of use, inhibitors are frequently employed[4,5]. Inhibitors are regularly utilized to stop the aggressive assault on metallic items and to stop metal disintegration and acid consumption. In the industrial setting, inhibitors are chemical substances that are employed in tiny amounts to slow down the rate at which metals and alloys corrode when exposed to harsh environments, and so reduce economic losses from metallic corrosion by delaying the corrosion process and limiting its rate. The way inhibitors work is heavily dependent on how they are formulated and how wisely they are used in certain situations. Researchers are looking at ecofriendly corrosion inhibitors since some unconventional materials can be utilized instead of synthesised, dangerous corrosion inhibitors. Due to the growing demand for green chemistry, the hunt for an effective inhibitor for metal corrosion in various corrosive conditions has recently gained increased importance[6-10].

Furthermore, the material to be employed as a metal corrosion inhibitor needs to be affordable, easily accessible, and ecologically friendly because the entire concept of metal protection is based on financial benefit and cological durability. Plants are a good source of inexpensive, easily accessible, and safe green inhibitors. Plant components have an organic composition and include specific phytoconstituents[11-15]. Numerous reports have indicated that plant extracts from diverse sections are good and efficient metal corrosion inhibitors in a variety of corrosive conditions such as *Hymenaeastigonocarpa fruit shell*[16], *Peganum harmala*[17], *Chrysophyllum albidum*[18], *Swertiachirata*[19], *Magnolia kobus*[20], *Dolichandra unguis-cati leaves*[21], *Plectranthus amboinicus*[22], *African mangosteen leaves*[23] their affordability and environmental friendliness make

them widely recognized on a global scale[24,25]. This study includes the plant used as a medicinal product Cycas inermis since its leaves included twelve components, 7 of which have been determined for the extremely first time for this species. From the species, extracts included 14 biflavonoids, 3-lignans, 3-flavan-3-ols, 2-flavone-C-glucosides, 2-nor-isoprenoids, and 1 flavanone[26,27]. All of the plant's components seem to have numerous applications including in common household items, traditional medicine, pharmacology, food preparation, and the detection of gastric cancer cell production, migration, and invasion[28]. This plant specifically possesses antioxidant and antibacterial properties in its leaves[29]. The *CILE* plant extract acts as a potent and eco-friendly green corrosion inhibitor. Recently, various methods have been devised for isolating plant components. Among these, the Soxhlet extraction method is the most efficient in terms of time and resource conservation. This approach is both cost-effective and proficient at separating solid materials from aqueous solutions, utilizing solvent reflux and siphoning to continuously isolate the pure solvent from the plant matter. The heated sample, placed on filter paper, interacts with the solvent. When the solvent level surpasses the siphon top, it is siphoned back. This cycle extracts portions of the material repeatedly, ensuring the solid substance remains pure and concentrated in the RB flask. Fig. 1 illustrates the whole process. In this research, the crude leaf extract of Cycas inermis proves superior to synthetic inhibitors due to its renewability, biodegradability, sustainability, and consistent composition and effectiveness.

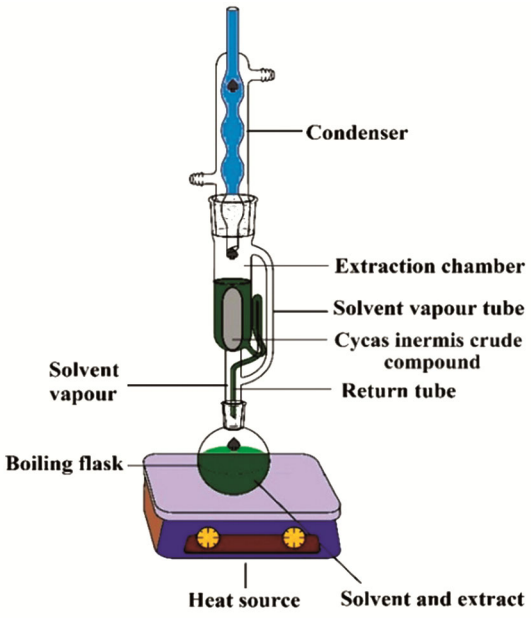

Fig. 1 — Soxhlet extraction technique

In order to extract *CILE* using the least quantity of solvent feasible, the Soxhlet extraction method was employed. Taking several electro-active components from the root of Cycas inermis and applying them as a possible corrosion inhibitor for SCS in 1 M H_2SO_4 is the primary goal of the current study.

Experimental Section

Soft cast steel coupons preparation

The SCS plate was cut into dimensions of 5 cm × 1 cm × 0.1 cm for the weight loss technique and 1 cm² for polarization studies. The chemical composition of the SCS was as follows (in percentage): Mn 0.27, Si 0.07, S 0.03, P 0.06, Ni 0.02, Cu 0.02, C 0.10, with the remainder being Fe. The samples were polished using silicon carbide papers ranging from 180 to 2000 grit, then degreased with acetone, rinsed with distilled water, and dried with a clean cloth. The initial weight of the samples was measured using an analytical balance.

Inhibitor preparation

The leaves of Cycas inermis were identified and collected from the campus of Karnatak Science College, Dharwad, India. Under running water, the leaves were washed and shade-dried for 8 days. The dried leaves were fine-grained using a mechanical grinder to convert the material into a powdered form. The Soxhlet process is a productive technique for extraction that involves continuously circulating the same solvent via the extractor. The technique of Soxhlet extraction is exceptionally inexpensive and only requires a small quantity of solvent. For this study, 25 g of powdered plant material was taken in the extractor and was extracted using 300 mL of ethanol and subjected for a period of 6 h. The extracted solution was then concentrated using a rotary evaporator. Subsequently, a specified amount of the crude extract was dissolved in ethanol to obtain the *CILE* stock solution.

Preparation of test solution

The samples are subjected to a corrosive solution consisting of a 1.0 M H_2SO_4 solution. An inhibitor solution was formed by diluting a different range of *CILE* solutions in 1 M H_2SO_4. Reagents of AR grade and double-distilled water were utilized to create corrosive liquid samples.

Mass loss measurements

Accurate measurements were taken of the initial weights of the pre-treated specimens, which were then fully submerged in 100 mL of an experimental solution containing 1 M concentration of H_2SO_4 both with and without varying doses of the inhibitor. These immersions occurred at different time intervals 1, 2, 3, 4, 5, 6 and 12 h, and were maintained at a constant temperature of 301 K. Subsequent to the designated exposure periods, the specimens were extracted, subjected to drying, and their weights were recorded once again. Utilizing the obtained weight differentials, the inhibition efficiency (η_W), surface coverage (θ), and deterioration rate (mmpy) were derived through the application of specific mathematical formulations.

Electrochemical studies

An electrochemical workstation, specifically the CH-Electrochemical model CH1660D, was utilized to perform the electrochemical measurements. The setup included a standard glass electrochemical cell configured with three electrodes. This cell was equipped with a platinum electrode serving as the counter electrode, a saturated calomel electrode (SCE) acting as the reference electrode, and a SCS sample with an uncovered surface area of 1 cm² clamped up in a specimen holder, functioning as the working electrode (WE). All potential values recorded during the measurements were referenced against the SCS.

Studies on Tafel polarization

A meticulously smoothened sample was exposed to a 1 M sulfuric acid solution as the deterioration medium, both without and with the inhibitor, at a temperature of 303 K. The sample was then left to reach a stable open-circuit potential (OCP). Once the OCP was established, the sample was polarized by applying a voltage of -200 mV in the cathodic direction and +200 mV in the anodic direction at a scan rate of 1 mV/s. This process was conducted to obtain the potentiodynamic current-potential curves.

Investigations using electrochemical impedance spectroscopy (EIS)

Impedance measurements were made between 0.01 Hz and 100 kHz at the open-circuit potential using a 5-mV AC sine wave voltage. Nyquist plots were used to analyze the impedance data, with the charge transfer resistance (R_{ct}) determined from the diameter of the semicircular arc in the plot.

Thermodynamic factors and adsorption isotherm

The impact of the *CILE* component that binds to the metal surface on the adsorption kinetics in a 1M H_2SO_4 solution was assessed across a temperature range of 301 to 321 ± 1K using conventional mass loss measurements. The thermodynamic aspects of the adsorption kinetics were thoroughly analyzed, and the collected data were fitted into the appropriate adsorption model to gain deeper insights into the process.

Surface investigations

The investigation into the alterations in the barrier morphology of SCS throughout the course of corrosion and protection processes was conducted using SEM, specifically employing the Model-JEOL JSM-IT 500LA instrument for atomic force microscopy (AFM-Nanosurf® EasyScan 2). FT-IR spectroscopy was employed to elucidate the chemical interactions involving the *CILE* functional group on the surface of SCS by utilizing a Nicolet 6700 spectroscope. Additionally, to assess the hydrophobicity of the metal surface, a WCA analysis was performed. This study was carried out using the Model-DMs-401 FAMAS software developed by Kyowa Interface Science Co. Ltd., Japan.

Results and Discussion

Results of weight loss assessment

The acid dissolution behavior of SCS in 1.0 M H_2SO_4 was examined using mass reduction and electrochemical techniques, both in the presence and absence of *CILE*. The SCS dissolution rate was found to be quite high when 1.0 M H_2SO_4 was used without inhibitor; however, the dissolution rate was significantly decreased when an inhibitor was added.

The dissolution rate and $\%\eta_W$ of SCS in an aqueous acid at 301 ± 1 K with various *CILE* doses and different time hours are shown in Table 1. Corrosion will occur more quickly in the absence of an inhibitor due to the plenty of H^+ ions available in the acid medium, which speeds up the reduction process. SCS corrosion is reduced by *CILE* in comparison to acidic media, and a raise in inhibitor concentration improves inhibitory efficacy. At an optimal *CILE* dose of 2.0 g/L for a 1.0 M H_2SO_4 solution, the highest efficiency of 96.15% was observed. 2.0 g/L was determined to be the ideal inhibitor dosage because no discernible increase in efficacy was seen when the inhibitor concentration was raised. If the concentration of the inhibitor is higher than 2.0 g/L, the inhibitor-metal connections may become weaker, and H_2O or SO_4^{2-} ions may replace the inhibitor, which will reduce the inhibitor's effectiveness.

Table 1 — Weight-loss details for SCS in 1M H_2SO_4 with and without *CILE* at 301 ±1K

Time (h)	Conc. (g/L)	Corrosion rate (mmpy)	Inhibition efficiency *(%η_W)*	Surface coverage (θ)
1	Blank	52.28		
	1.25	5.03	90.38	0.9038
	1.50	4.02	92.30	0.9230
	1.75	3.02	94.23	0.9423
	2.0	2.01	96.15	0.9615
2	Blank	40.72		
	1.25	4.52	88.89	0.8889
	1.50	3.52	91.36	0.9136
	1.75	3.02	92.59	0.9259
	2.0	2.01	95.06	0.9506
4	Blank	37.20		
	1.25	4.02	89.19	0.8919
	1.50	3.27	91.22	0.9122
	1.75	2.51	93.24	0.9324
	2.0	2.01	94.59	0.9459
5	Blank	34.58		
	1.25	4.42	87.21	0.8721
	1.50	3.82	88.95	0.8895
	1.75	3.22	90.70	0.9070
	2.0	2.61	92.44	0.9244
6	Blank	32.51		
	1.25	4.19	87.11	0.8711
	1.50	3.69	88.66	0.8866
	1.75	3.18	90.21	0.9021
	2.0	2.68	91.75	0.9175
12	Blank	33.68		
	1.25	3.52	88.56	0.8856
	1.50	3.27	89.55	0.8955
	1.75	3.02	90.30	0.9030
	2.0	4.61	91.04	0.9104

In an acidic solution, the liberation of hydrogen also continues to be dominant. Therefore, mass accumulation is not occurring throughout the superficial layer of SCS. In an acidic solution, the *CILE* constituents undergo protonation, which results in a decrease in the reduction reaction. When *CILE* components are added, they attach to the soft cast steel's surface and form a thin coating that keeps the metal surface isolated from acidic environments and prevents corrosion. Eqs (1), (2), and (3) were used, accordingly, to quantify the corrosion rate (υ_{corr}), the percentage of inhibitory efficacy *(%η_w),* and the surface coverage (θ) of the *CILE* plant extract[30].

$$W_{corr} = \frac{87.6 \times W_2 - W_1}{ATD} \quad \text{... (1)}$$

Where A is the exposed surface area for corrosion investigations in square centimeters, T is the immersion duration in h, D is the density of the SCS sample (7.85 g/cm^3), and W_2-W_1 is the observed weight loss in mg. The following formula was used to calculate the surface coverage (θ) and percentage inhibitory effectiveness *(%η_w)*:

$$\%\eta_p = \frac{W_2 - W_1}{W_2} \times 100 \quad \text{... (2)}$$

$$\theta = \frac{W_2 - W_1}{W_2} \quad \text{... (3)}$$

Where, W_2 and W_1 are the mass loss of SCS bare and with inhibitor.

The changing protection ability of the corrosion inhibitor over time is a critical aspect of the study. Table 1 illustrates this phenomenon in detail, showing how the inhibition efficiency evolves with prolonged exposure. Initially, the inhibition efficiency is high due to the rapid adsorption of *CILE* molecules on the SCS surface, forming a protective film. However, over time, there is a gradual decrease in inhibition efficiency. The decline in protection efficiency can be attributed to several factors. As time progresses, the concentration of active *CILE* molecules in the solution may reduce due to continuous adsorption and possible degradation, leading to a thinner protective layer. Additionally, the formation of corrosion products on the SCS surface can impede further adsorption of inhibitor molecules, thus reducing the effectiveness of the protective film. Variations in temperature and pH over time can also affect the stability and adsorption efficiency of the inhibitor molecules[31].

Potentiodynamic polarisation measurements

The polarization curves of SCS in a 1.0 M H_2SO_4 solution are displayed in Fig. 2 both in the absence and with various inhibitor concentrations. Eq. (4) is utilized to calculate the inhibition efficiency for each inhibitor concentration.

$$\%\eta_w = \frac{i^o_{corr} - i_{corr}}{i^o_{corr}} \times 100 \quad \text{... (4)}$$

Here, i^o_{corr} and i_{corr} symbolize corrosion current densities without and with various *CILE* doses. Table 2 lists the electrochemical characteristics, including cathodic (β_c) and anodic (β_a) Tafel plots, inhibition efficiency *(%ηp)*, corrosion potential (E_{corr}), and corrosion current density (icorr). Each experiment was conducted three times for each test group under identical conditions. The consistency of the results was confirmed by the standard deviation of the electrochemical polarization measurements. Lower corrosion current densities are achieved by raising inhibitor concentrations. Fig. 2 and Table 2 clearly demonstrate that the presence of *CILE* in the acidic medium progressively reduces both cathodic and

Table 2 — Soft cast steel corrosion characteristics were measured at 301±1K in 1M H_2SO_4 using the potentiodynamic polarization technique

Conc. *(g/L)*	E_{corr} *(V vs SCS)*	I_{corr} *(A cm^{-2})*	β_a *(V/dec)*	$-\beta_c$ *(V/dec)*	*C.R. (mil/yr)*	*(%η_w)*
Blank	-0.525	2.637×10^{-3}	7.095	5.721	1.207×10^{3}	
1.25	-0.482	4.243×10^{-4}	10.386	7.732	1.942×10^{2}	83.91
1.5	-0.480	3.180×10^{-4}	11.293	7.761	1.456×10^{2}	87.94
1.75	-0.484	2.066×10^{-4}	11.813	7.923	9.457×10^{1}	92.17
2.0	-0.481	1.665×10^{-4}	12.178	7.826	7.619×10^{1}	93.69

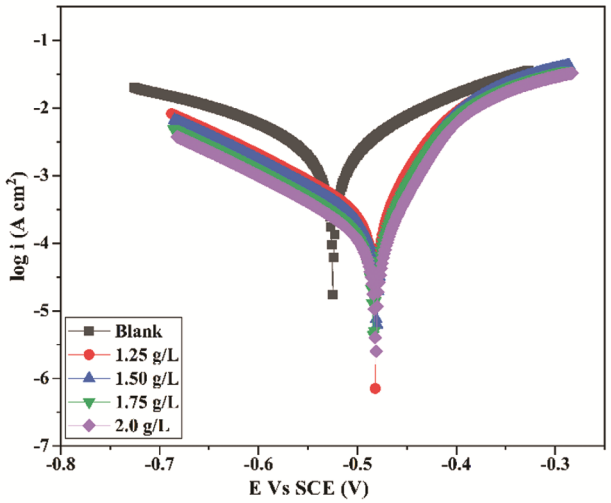

Fig. 2 — Soft cast steel polarization curves at various CILE concentrations

anodic current densities. This effect becomes increasingly pronounced with higher concentrations of *CILE*[32,33]. This behaviour demonstrates the inhibitor's ability to prevent SCS corrosion in acidic medium and by chemically adsorbing its molecules on both anodic and cathodic sites, which facilitates that it functions through a mixed mode of inhibition. Table 2 shows the relationship between inhibitor concentration and the decrease in corrosion current density. Fig. 2 illustrates that the presence of an inhibitor causes a significant shift in both cathodic and anodic polarization curves toward lower current densities. This shift is more pronounced in the cathodic Tafel curves due to the inhibitor reducing hydrogen evolution, and in the anodic Tafel curves due to decreased metal dissolution. These findings indicate effective corrosion mitigation. From Table 2, it is evident that the presence of the inhibitor significantly reduces both the anodic Tafel slopes and cathodic Tafel slopes indicating that the inhibitor shows mixed behaviour[34,35]. The reduction in the corrosion rate for soft cast steel when an inhibitor is added to the corrosive medium supports this conclusion. The data in Table 2 elucidates that as the inhibitor concentration increases, the corrosion rate of the metal decreases in 1M H_2SO_4 at a temperature of 301 ± 1 K. These results prompt the inference that *CILE* holds promise as a potent inhibitor. The examined inhibitors appear to behave as mixed-type agents, according to the overall data. It has been noted that when inhibitor concentrations rise, inhibition efficiency also increases. Maximum inhibitory efficiency is achieved at a concentration of 2.0 g/L, with a maximum value of 93.69%.

Electrochemical impedance spectroscopy measurements

An essential non-destructive technique for evaluating the protective layer that develops on metallic surfaces and providing an estimate of the mechanism causing corrosion are done by electrochemical impedance spectroscopy measurement. EIS studies enable a quantitative comprehension of the kinetics of the electrode process and the surface characteristics at the metal/solution contact. EIS provides a quick and simple method for monitoring the track of corrosion processes, with evaluation carried out close to the corrosion potential to ensure accurate results[36]. The fact that EIS operates at lower applied voltage levels makes non-destructive tests possible. Nyquist plots of the EIS results for soft cast steel subjected to 1 M H_2SO_4 solution at 301 ± 1 K, both with and without varying concentrations of *CILE*. Z-simp 3.21 was used to generate the equivalent circuit R(QR(LR)), are shown in Fig. 3. The adsorption of elements such as $(H^+)_{ads}$ and $(SO_4^{2-})_{ads}$ is what allows the LF inductive loop to relax. In the present research, various impedance variables, such as the constant phase element (CPE) takes on a double-layer capacitance for bettering the circuit's fit double layer capacitance, solution resistance (R_s), n is the phase shift, (R_L) inductive resistance, charge transfer resistance (R_{ct}), percentage inhibition efficacy *(%η_p)* and L represents the inductive element were calculated from fitting curves. Table 3 summarizes the results that were achieved. The following equation was then used to calculate capacitance and *(%η_p)* values:

$$Z_{CPE} = \frac{1}{Y_o(j\omega^n)} \quad \ldots (5)$$

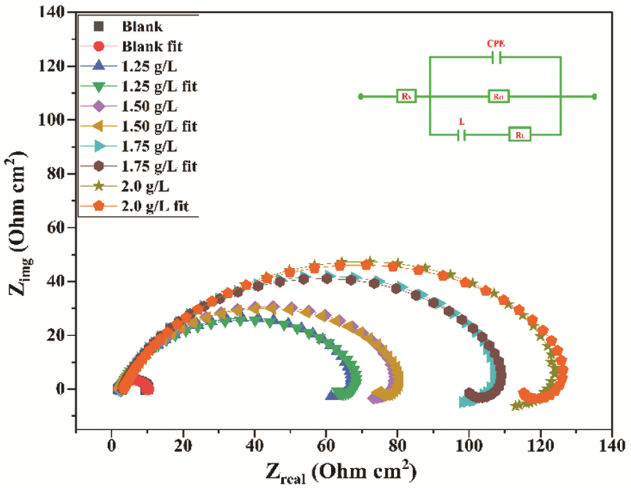

Fig. 3 — Nyquist plots for SCS in the nonexistence and existence of CILE

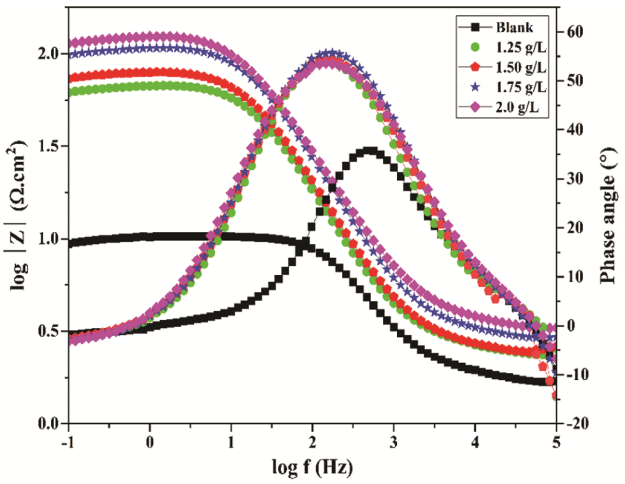

Fig. 4 — Bode plots showing the effects of adding and without adding CILE

Table 3 — The electrochemical characteristics of SCS samples were examined by adding *CILE* and in bare condition.

Concentration (g/L)	R_s (Ω cm^2)	$Y_0 \times 10^{-6}$ ($S\ s^n\ cm^{-2}$)	*N*	R_p (Ω cm^2)	C_{dl} ($\mu F/cm^{-2}$)	*L* (Ω cm^2)	R_L (Ω cm^2)	($\%\eta_p$)
Blank	1.77	292.0	0.83	8.748	180.84	32.7	81.2	
1.25	2.49	287.5	0.81	70.01	169.34	119.4	451.7	87.50
1.50	2.52	263.6	0.80	82.02	156.37	216.5	578.9	89.33
1.75	3.36	222.1	0.77	112.5	120.83	210.3	704.4	92.22
2.0	2.99	195.6	0.80	133.2	116.05	222.2	704.6	93.43

Where, Y_o= CPE values, n = CPE exponent acquired from the Phase shift value, ω = is angular frequency, where, $\omega = 2\pi f$, f = is the frequency, j = imaginary part[37].

$$\%\eta_p = \frac{R_{ct} - R_{ct}^o}{R_p} \times 100 \quad \ldots (6)$$

According to the information provided, the solution resistance (R_s), which signifies the total opposition of the electrode and substance, remains almost unchanged in 1M H_2SO_4 solution with and without *CILE* extract. Conversely, the charge transfer resistance (R_{ct}) values are depicted as semicircles centered on the real axis of the Nyquist diagram. It has been observed that the charge transfer resistance value increases considerably after adding various amounts of *CILE*. The *CILE* plant extract's inhibitory effect was ascertained by applying the inverse correlation between the corrosion current density and the (R_p) value.

Where 'n' represents the CPE, the exponent obtained from the phase shift value. Here, the CPE exponent values vary from -1 to 0 to +1. When n = 1, the CPE can behave like an inductor, while n = 0 means that the CPE can behave like a resistor. The impedance of the CPE shows up when n = 0.5 and n = -1, then the CPE can act as a capacitor. Here obtained n values are presented in Table 3, which indicates that the values of n are slightly less than one, which shows that the CPE is slightly different from the capacitor[38]. Further, when the extract molecules are present on the SCS surface, there is an increase in R_{ct} values, indicating that the inhibitory efficacy of the extract is via an adsorption mechanism. Fig. 4 shows the Bode plot that relates the logarithm of impedance and phase shifting to the logarithm of the frequency. In bode graphs, the lowest phase angle and impedance data suggest severe corrosion on the exposed metal surface[39]. The *CILE* extract has a maximal inhibitory activity of 93.43% at 2.0 g/L and functions effectively as a corrosion inhibitor to mitigate corrosion on SCS. A 3-D graph is given in Fig. 5 to illustrate the relationship of $\%\eta_p$ for mass loss, potentiodynamic polarization tests, and EIS measurements.

Impact of temperature

The experiment covered a range of temperatures, from 301 K to 321 ± 1K, showing a consistent trend at higher temperatures that led to increased corrosion rates and reduced inhibition efficiency. The phenomena are particularly apparent in acidic environments where the evolution of H2 gas predominates because anodic and cathodic processes are accelerated by high temperatures. The impact of temperature on inhibition

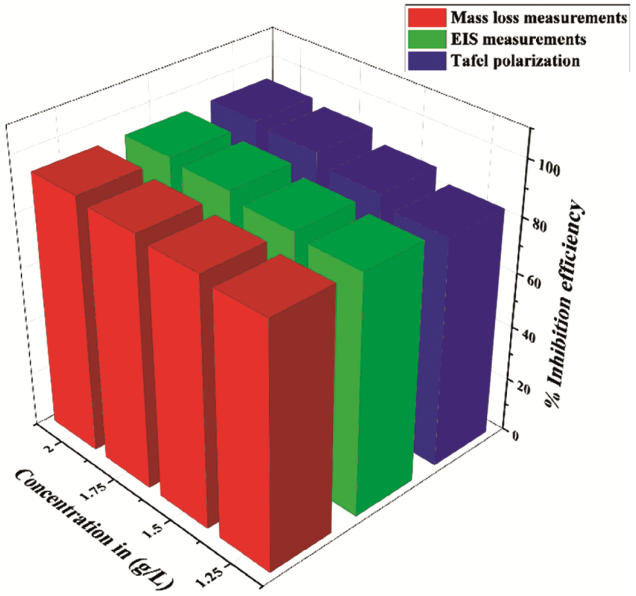

Fig. 5 — 3-D graph of the $\%\eta_p$ of weight loss measurements, PDP studies and EIS

Table 4 — Effect of The temperature on SCS in 1M H_2SO_4 with varying doses of *CILE*

Temp. *(K)*	Concentration *(g L^{-1})*	Corrosion rate *(mm/year)*	Percentage inhibition efficiency *(%η_p)*	Surface coverage *(θ)*
301	Blank	52.28		
	1.25	5.03	90.38	0.9038
	1.50	4.02	92.30	0.9230
	1.75	3.02	94.23	0.9423
	2.0	2.01	96.15	0.9615
306	Blank	84.45		
	1.25	10.05	88.09	0.8809
	1.50	8.04	90.48	0.9048
	1.75	6.03	92.86	0.9286
	2.0	5.03	94.05	0.9405
311	Blank	113.60		
	1.25	16.09	85.84	0.8584
	1.50	13.07	88.50	0.8850
	1.75	10.05	91.15	0.9115
	2.0	9.05	92.03	0.9203
316	Blank	145.77		
	1.25	26.14	82.07	0.8207
	1.50	23.12	84.14	0.8414
	1.75	20.11	86.21	0.8621
	2.0	17.09	88.28	0.8828
321	Blank	170.91		
	1.25	35.19	79.41	0.7941
	1.50	31.17	81.76	0.8176
	1.75	27.14	84.12	0.8412
	2.0	23.12	86.47	0.8647

effectiveness is explained in Table 4, which compares situations under which there is inhibition and those under which there is no inhibition at various doses of *CILE*. Table 4 presents data indicating a clear

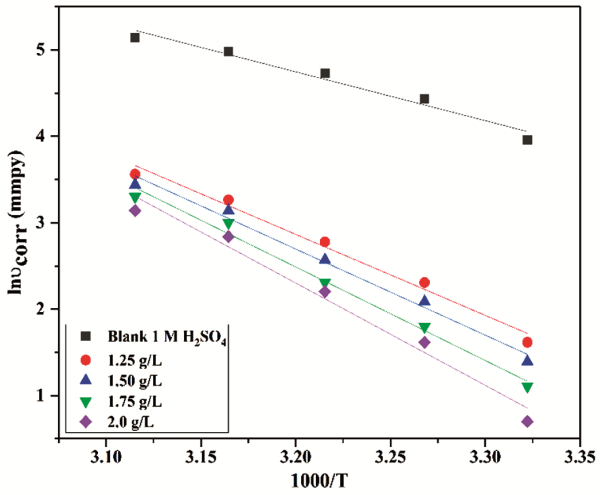

Fig. 6 — Arrhenius diagrams for SCS

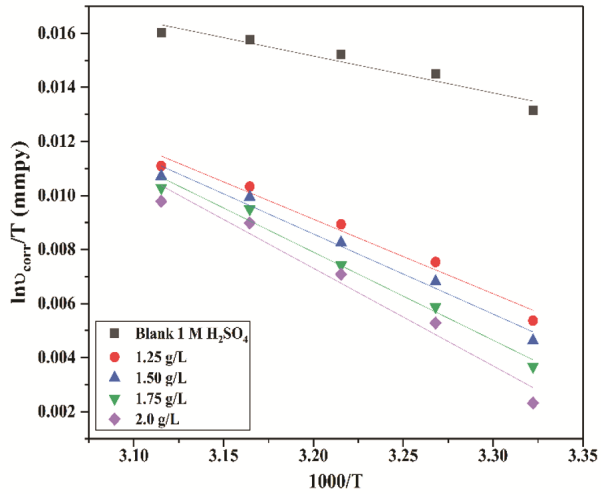

Fig. 7 — Transition state diagrams for SCS

Table 5 — *CILE* inhibitor activation characteristics for SCS

Conc. (g/L)	*Ea* (kJ mol^{-1})*	*A (kJ mol^{-1})*	*ΔH* (kJ mol^{-1})*	*ΔS* (J mol^{-1} K^{-1})*
Blank	46.99	8.27×10^{9}	113.24	-23.701
0.975	78.05	1.95×10^{14}	229.47	-23.663
1.200	82.95	1.09×10^{15}	246.59	-23.656
1.350	90.04	1.35×10^{16}	271.20	-23.647
1.500	98.42	2.83×10^{17}	300.38	-23.637

correlation between temperature and corrosion rate. This indicates that the protective inhibitor coating on SCS surfaces has been compromised, resulting in desorption at elevated temperatures[40].

Figs 6 and 7 graphically represent the Arrhenius and transition state conditions for SCS in a 1.0 M H_2SO_4 solution at various concentrations of the *CILE* inhibitor. The activation factors are explained in Table 5 and Eq. (7) represents the expression for the Arrhenius and transition state formulas[41].

$$lnv_{corr} = lnA - \frac{E_a^*}{RT}, \quad \text{... (7)}$$

Within the Arrhenius equation, A symbolizes the pre-exponential constant, R stands for the gas constant, and T represents the absolute temperature. According to the information in Table 5, the inhibited system demonstrates a greater activation energy (E_a) value of 98.42 kJ/mol, whereas the uninhibited system has a lower value of 46.99 kJ/mol. It is important to remember that a rise in the *CILE* concentration leads to a noticeable rise in E_a, which was attributed to chemical adsorption phenomena. The activation enthalpy (ΔH*) and entropy (ΔS*) were then computed using Eq. (8) in accordance with the Arrhenius equation.

$$ln\frac{v_{corr}}{T} = \left[ln\frac{R}{Nh} + \frac{\Delta S^*}{R}\right] - \frac{\Delta H^*}{RT}, \quad \text{... (8)}$$

According to the Arrhenius equation, which takes into account A as the pre-exponential constant, R is the gas constant, and T as the absolute temperature. This increased E_a corresponds to the higher concentration of *CILE*, which is thought to be due to chemical adsorption. The Arrhenius plot, which shows the relationship between lnv_{corr} vs *1000/T* (as displayed in Fig. 6), is exhibiting a linear correlation with a slope equivalent to (E_a/2.303R). When plotting lnv_{corr}/T vs *1000/T* (as displayed in Fig. 7), an erect line is created, where the slope represents (ΔH*/2.303R), and the intercept is [ln(R/Nh) + (ΔS*/2.303R)]. These graphical representations aid in determining the activation entropy (ΔS*) and activation enthalpy (ΔH*)[42].

Without the use of an inhibitor, the activation enthalpy (ΔH*) in aqueous H_2SO_4 were calculated to be 113.24 kJ/mol to 300.38 kJ/mol, correspondingly. Localized corrosion at surface sites with greater E_a* is suggested by the greater E_a* and ΔH* data in the presence of the inhibitor, which point to an increased energy barrier. While ΔS* levels are linked to greater disorderliness during the inhibitor's adsorption and subsequent attachment to the soft steel surface, positive ΔH* values indicate suppressed corrosion. A raised ΔS* and enhanced solvent entropy are resulting from the displacement of H_2O molecules by this adsorption[43,44].

Behaviour of adsorption isotherms

The prevailing assumption is that the process of corrosion inhibition occurs as a result of the inhibitor constituents binding to the interface between the metal barrier and the surrounding solution. Although the corroding surface adsorption process never reaches an equilibrium state, it does so at a stable adsorption rate that is noticeably high. In this nearly static process, the thermodynamic analysis of quasi-equilibrium adsorption is justified, employing suitable equilibrium isotherms. The efficacy of the *CILE* as an inhibitor hinge on its capacity to adhere to the metal barrier. Gaining insight into the manner of adsorption is essential for understanding the correlation between the inhibitor and the metal barrier[45]. The application of the Langmuir adsorption isotherm to experimental data insights into accumulation of the *CILE* on SCS in aqueous acid at a temperature of 301 ± 1K. The Langmuir isotherm offers the most accurate match and exhibits impressive agreement with the given Eq. (9).

$$\frac{C}{\theta} = \frac{1}{K_{ads}} + C, \quad \text{... (9)}$$

The Langmuir adsorption isotherm equation achieved remarkable success in fitting the model, with C representing concentration, θ denoting surface area coverage, and K_{ads} as the adsorption equilibrium constant.

The effectiveness of utilizing the Langmuir adsorption isotherm to study inhibitor constituent's adsorption on SCS surfaces is demonstrated by the correlation factor (R^2) and a slope value close to unity. This implies that the molecules that have been adsorbed do not interact with one another. Table 6 presents the adsorption equilibrium constants (K_{ads}) derived from the linear plots of inhibitor concentration (C_{inh}) versus the ratio of inhibitor concentration to surface coverage (C_{inh}/θ), as depicted in Fig. 8, which includes error bars for accuracy. These findings suggest a stronger and more efficient interconnection between the metal barrier and the *CILE* compounds under investigation[46]. Additionally, Table 6 furnishes the data for the standard free energy of adsorption (ΔG^o_{ads}), which is linked to K_{ads} by a pertinent Eq. (10).

$$\Delta G^o_{ads} = -2.303RTlog\left(K_{ads} \times C_{H_2O}\right), \quad \text{... (10)}$$

Table 6 — Data of the thermodynamics of inhibitor adsorption on SCS surface at varying temperatures in 1.0 M H_2SO_4.

Temp. (K)	K_{ads} ($L\ mg^{-1}$)	ΔG^0_{ads} ($kJ\ mol^{-1}$)	ΔH^0_{ads} ($kJ\ mol^{-1}$)	ΔS^0_{ads} ($J\ mol^{-1}\ K^{-1}$)
301	4418.33	-31.061	-16.77	47.48
306	4082.80	-31.377	-16.77	47.74
311	3750.23	-31.699	-16.77	48
316	3425.71	-31.941	-16.77	48.01
321	2856.57	-31.961	-16.77	47.32

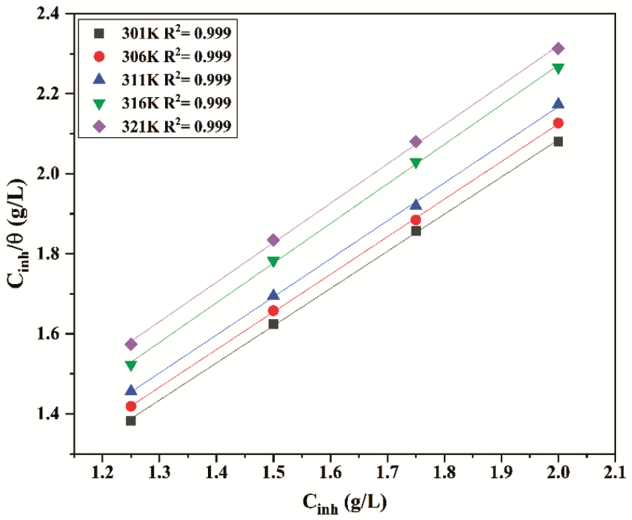

Fig. 8 — Graphs illustrating the Langmuir Adsorption Isotherm for SCS immersed in a 1.0 M H_2SO_4 solution at varying inhibitor concentrations within the temperature range of 301-321 ± 1 K

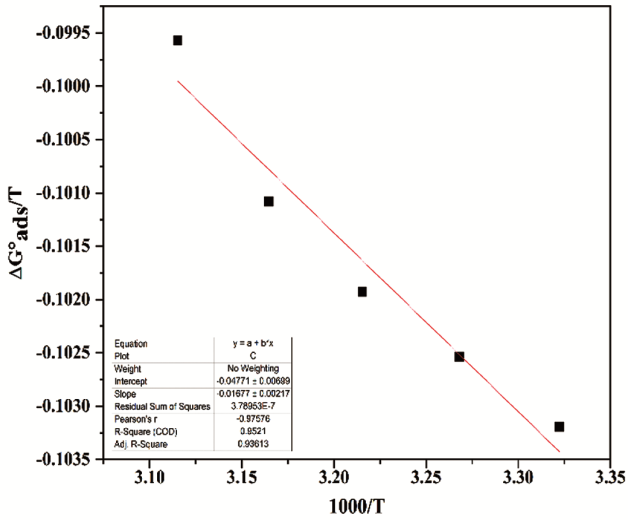

Fig. 9 — Graph of $\Delta G^o_{ads}/T$ versus 1000/T for 1 M H_2SO_4

Investigations into the interactions between the *CILE* and the analysis of adsorption-free energy (ΔG^o_{ads}) on the barrier of SCS often demand careful consideration. The connection between ΔG^o_{ads} and the equilibrium constant for the adsorption process (K_{ads}) is described by the above equation. Here R denotes the gas constant, T the temperature, and C_{H2O} the water content. To find the enthalpy of adsorption (ΔH^o_{ads}), the slope data ofΔG^o_{ads}/T vs. 1000/T were used in Fig. 8. Furthermore, the Eq. (11) is utilized to compute the entropy of adsorption (ΔS^o_{ads}) as follows:

$$\Delta S^o_{ads} = \frac{(\Delta H^o_{ads} - \Delta G^o_{ads})}{T}, \quad \ldots (11)$$

The adsorption process's thermodynamic parameters can be calculated using the above formulas. These metrics give crucial details regarding the strength and intensity of the *CILE*'s interaction with the metal barrier at different temperatures. Table 6 displays the determined values of ΔG^o_{ads} and K_{ads},. A ΔG^o_{ads} value below zero suggests that the accumulation of the *CILE* onto the SCS barrier occurs spontaneously. By applying this Eq. 1, determined value of ΔG^o_{ads} is -31.961 kJ/mol to -31.061 kJ/mol. The negative ΔG^o_{ads} value indicates that *CILE* molecules spontaneously self-adsorb onto the soft cast steel surface. This behaviour is consistent with the general tendency of organic inhibitors to self-adsorb on metal surfaces. If the ΔG^o_{ads} value is greater than -40 kJ/mol, chemical adsorption is considered predominant, whereas if it is less than -20 kJ/mol, physical adsorption is dominant. Values of ΔG^o_{ads} between these ranges indicate that both adsorption processes may occur. However, it is important to note that the adsorption of organic molecules on metal surfaces often involves a combination of both chemical and physical interactions. The ΔG^o_{ads} value for *CILE* is between these two extremes indicating that the adsorption involves both chemical and physical interactions. The initial stage in the adsorption of organic molecules from the extract involves their physical interactions with the electrode surface. These interactions occur through weak forces, such as dipole-dipole interactions. Beyond physisorption, chemical reactions may also take place. Chemical interactions can occur through charge sharing between the d orbitals of the metal and the free electron pairs of adsorption-active centers, such as nitrogen, sulfur, and oxygen atoms, as well as the π electrons of double or triple bonds in organic molecules. These findings indicate that the accumulation of the inhibitor on the SCS barrier involves a combination of physical and chemical adsorption characteristics. This underscores the intricate nature of the adsorption process, highlighting the contribution of various mechanisms to corrosion inhibition. Fig. 9 represents the adsorption enthalpy ΔH^o_{ads} (-16.77 kJ mol^{-1}) is negative, indicating the *CILE* adsorption is exothermic. The values of ΔS^o_{ads}that have been found are positive, signifying that the *CILE* components were adsorbed on the SCS surface by the desorption of water molecules which in turn improved the disorder and raised the entropy for adsorption[47-49].

Examining FT-IR spectra

The FT-IR spectrometer is an influential tool utilized to discern the bonding nature of organic inhibitors adhered to metal surfaces. FTIR spectra are utilized for scrutinizing the protective layer established on metal surfaces[50]. The suppression observed in the *CILE* could be attributed to the existence of these primary compounds, which possess functional groups as illustrated in Fig. 10. In this, infrared band of -OH detected at 3419 cm^{-1}, C-H stretching frequency of alkene at 2854 and 2922 cm^{-1},, C=O band of conjugated acid at 1663 cm^{-1}. The peak at 1380 cm^{-1} is due to -C-O stretching. The FT-IR spectrum of the SCS specimen after being immersed in an aqueous acid for 20 h, which includes 2.0 g/L of *CILE*, is illustrated in Fig. 10. It showed the stretching band of -OH at 3342 cm^{-1}, C-H stretching at 2973 cm^{-1}, C=O stretching vibration at 1650 cm^{-1} indicating that only these electron-donating centers of *CILE* constituents engage in interactions with the metallic substrate. The observed alterations in the stretching frequencies indicate that inhibitory molecules interact with the metal substrate through two possible mechanisms: chemical bond formation and weak intermolecular interactions. Based on FT-IR findings, the inhibitor compounds are made up of heteroatoms, which will function as Lewis bases and coat the metal substrate by forming a protective layer to minimize corrosion[50].

Scanning electron microscopy

The SEM is the best tool for acquiring insights into the inhibitor's effectiveness in safeguarding electrode barriers from significant harm and promoting the development of shielding layers on metal substrates. The examination was carried out on specimens immersed in acidic solutions, with the addition and non-addition of the *CILE* for a period of 24 h. Figs 11a,

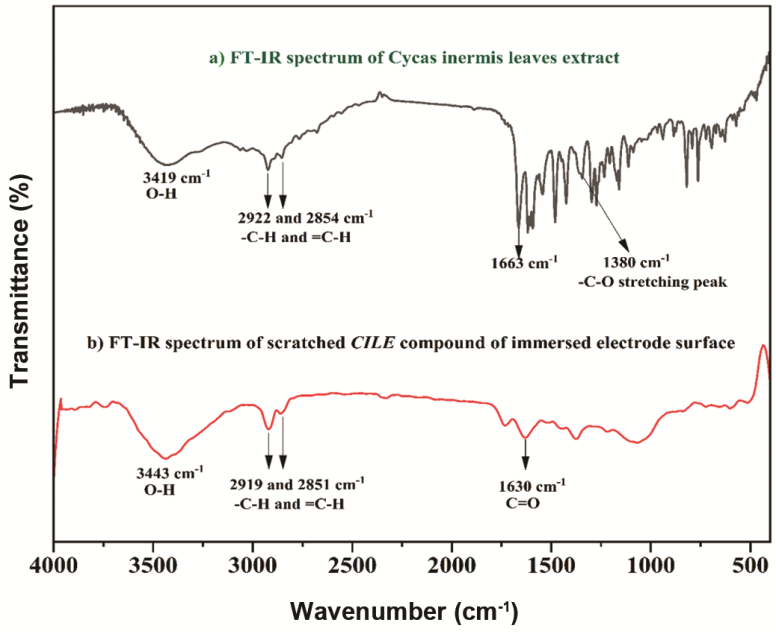

Fig. 10 — FTIR spectra of (a) Pure CILE and (b) SCS specimen immersed in acid containing 2.0 g/L CILE

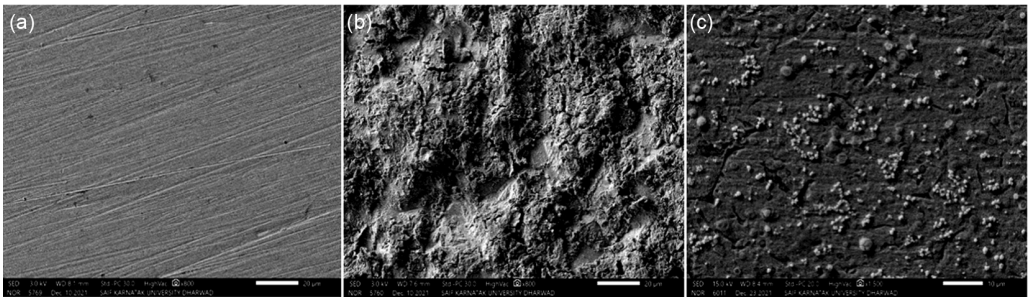

Fig. 11 — SEM pictures of SCS (a) Highly polished surface, (b) During submerged time of 24 h in aqueous acid i.e., 1M H_2SO_4 and (c) dipped time of 24 h in 1M H_2SO_4 with 2.0 g/L of CILE

11b and 11c showcase a sequence of SEM visuals. Fig. 11a illustrates the polished soft cast steel surface, exhibiting clarity and highlighting the consistent and flawless quality of the metal sample. In contrast, Fig. 11b depicts the SCS specimen exposed to an aggressive environment (i.e., lacking inhibitor), revealing superficial degradation and the presence of cavities resulting from the aggressive acidic medium attack. The SCS specimen suspended in the acidic solution containing the optimal inhibitor concentration of 2.0 g/L of *CILE* is represented in Fig. 11c. The metal superficial shows noticeably reduced damage, attributed to the formation of corrosion products formed amid the iron atoms and the *CILE* constituents, serving as a safeguard. Furthermore, this safeguard decelerates the corrosion mechanism by obstructing additional acid solution attacks on the SCS substrate, as a result diminishing the corrosion rate[51].

Atomic-microscope analysis

AFM stands out as an invaluable instrument for comprehending surface morphology across nano-to microscales, as well as for evaluating inhibitor effectiveness at metal-solution interfaces. AFM was used for post-experiment analysis of the surface morphology. To systematically examine the superficial texture of SCS with the existence and non-existence of the *CILE* inhibitors, we have captured AFM topographic images, displayed in Fig. 12a, b, and c, along with the corresponding outcomes in Table 7. Fig. 12a displays an AFM image of a highly smoothened SCS substrate, which shows the least R_a value of 22.627 nm. Fig. 12b displays the AFM image of the SCS sample without the *CILE* inhibitor in a corrosive environment, revealing a notably elevated R_a value of 241.4 nm. In Fig. 12c, the AFM image depicts the soft cast steel surface when exposed to an optimal concentration of 2.0 g/L of *CILE* inhibitor. Table 7 reveals the average roughness of the samples. The observation explains the significant improvement in surface smoothness, as evidenced by the reduction in the value of R_a to 81.541 nm. These findings indicate that the acid environment caused serious harm to the SCS substrate when the *CILE* was absent. However, in the existence of the *CILE*, the acid environment only caused minor damage to the SCS barrier. This demonstrates that the *CILE*'s active components are intended to adhere to the SCS barrier, reducing the corrosion rate[52,53].

Contact angle analysis

To assess how the soft cast steel surface behaves in terms of its hydrophobic and hydrophilic properties, a contact angle experiment was conducted with and without the *CILE.* Fig. 13a depicts the samples dipped in the aggressive solution without the inhibitor at about 6 h, displaying a contact angle of 41.5 degrees, indicating its hydrophilic nature. Fig. 13b demonstrates that the contact angle on the SCS surface rises when a minimal dose of the inhibitor is added, specifically at 1.25 g/L, with the contact angle reaching 100.3°. This indicates that the components within *CILE* effectively bond to the SCS. In Fig.13c, for the optimized *CILE* dose of 2.0 g/L, the contact angle rise to 112.9°. The increase in contact angle values suggests that the hydrophilic character of the

Table 7 — AFM results on the *SCS* surface in 1M H_2SO_4 in presence and absence of *CILE*

Specimen	Conc. (g/L)	Average roughness (Ra) (nm)	Root mean square roughness (Sq) (nm)
Polished	-	22.627	28.507
Blank 1 M H_2SO_4	-	241.4	294.28
Inhibitor	2.0	81.541	109.32

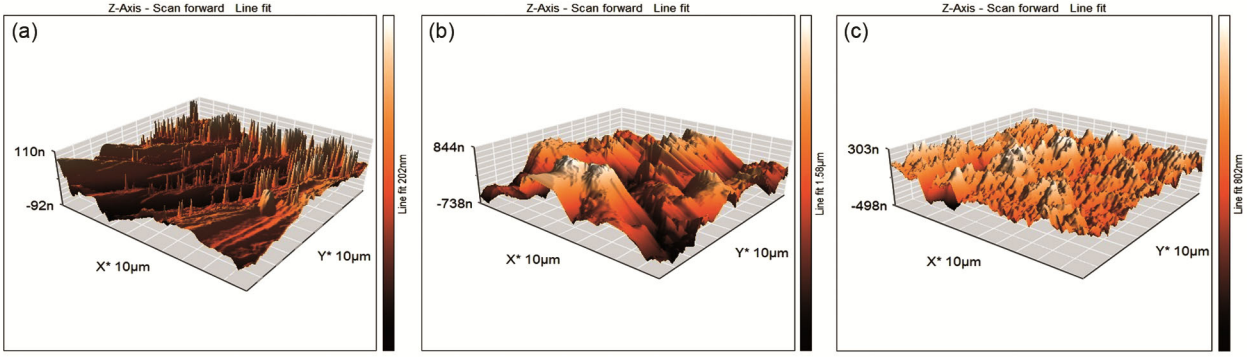

Fig. 12 — atomic force microscopy 3-D micrographs of (a) polished SCS surface, (b) SCS dipped for 6 h in aqueous acid and (c) SCS in acid along with 2.0 g/L of CILE

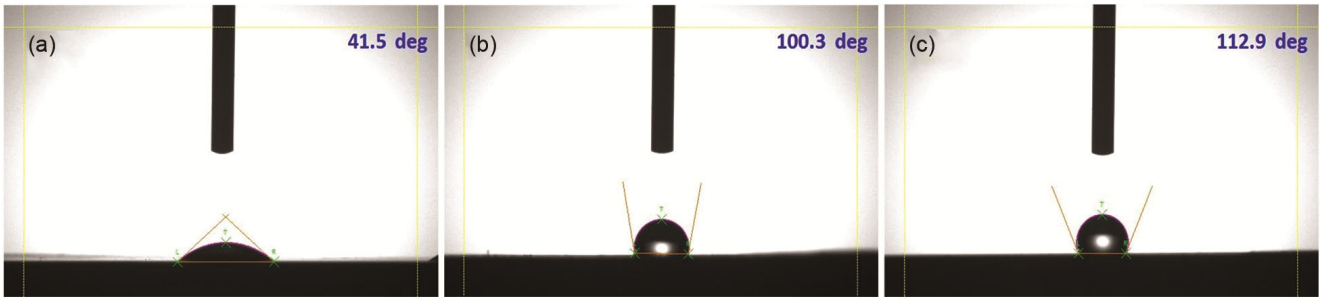

Fig. 13 — Contact angle studies on SCS surface with 6 h immersion time: (a) sample dipped in acidic solution without CILE (b) Immersion of SCS in corrosive medium with 1.25 g/L CILE and (c) immersion of SCS in 1M H_2SO_4 containing a 2.0 g/L CILE

soft cast steel surface is reduced. This alteration is caused by *CILE*'s organic components sticking to the soft cast steel surface and obstructing its active areas. Consequently, the rise in hydrophobicity points to a drop in soft cast steel corrosion rates[54-60].

Conclusion

Considerable investigation has been conducted using diverse approaches to examine the corrosion inhibitive characteristics of the *CILE* inhibitor, aiming to mitigate the corrosion of soft cast steel in a 1M H_2SO_4 solution. The inhibition efficiency was thoroughly assessed using the weight loss method, potentiodynamic polarization, and electrochemical impedance spectroscopy techniques. Electrochemical analysis revealed that *CILE* functions as a potent corrosion inhibitor for SCS and inhibition efficiency increases with increase in *CILE* concentration. The maximum inhibition efficiency obtained from the weight loss method, polarization technique, and electrochemical impedance spectroscopy were 96.15%, 93.69%, and 93.43%, respectively. According to Tafel graphs, *CILE* acts as a mixed-type inhibitor, regulating the corrosion rate of both cathodic and anodic reactions. EIS studies unveiled a rise in charge transfer resistance in the presence of *CILE*. The adsorption mechanism of *CILE* on the SCS surface follows the Langmuir adsorption model, and the values of the corrosion protection effect at higher temperatures, activation energy, and enthalpy indicate that both physisorption and chemisorption are involved in the adsorption process. Analysis using FT-IR, SEM, and AFM indicated that *CILE* safeguards the soft cast steel surface by creating a protective layer on the specimen surface, consistent with the electrochemical data. The contact angle evaluation illustrated that *CILE* constituents render the specimen surface hydrophobic. In conclusion, *CILE* exhibits excellent corrosion inhibition properties for SCS in a 1M H_2SO_4 solution, making it a viable candidate for industrial applications where sustainable and effective corrosion protection is required.

Conflict of interest

The authors declare no conflict of interest.

References

1 Deyab M A, Corrosion inhibition of aluminum in biodiesel by ethanol extracts of Rosemary leaves, *J Taiwan Inst Chem Eng*, 58 (2016) 536.

2 Hsissu R, Benassaoui R, Benhiba F, Hajjaji N & Elharfi A, Application of a new tri functional epoxy prepolymer: Triglycidyl ether ethylen of bisphenol a (TGEEBA) in the coating of E24 steel in NaCl 3.5%, *J Chem Technol Metall*, 52 (2017) 431.

3 Athira R, Poongothai N, Neena P K, Babu T G S & Stanley J, Study of corrosion protection effect of low cost bio extract - polymer coating material for mild steel in acidic and marine environments - a cost effective approach, *Int J Eng Technol*, 7 (2018) 315.

4 Hsissou R, Bekhta A, Elharfi A, Benzidia B & Hajjaji N, Theoretical and electrochemical studies of the coating behavior of a new epoxy polymer: Hexaglycidyl ethylene of methylene dianiline (HGEMDA) on E24 steel in 3.5% NaCl, *Port Electrochim Acta*, 36 (2018) 101.

5 El-Lateef A & Hany M, Experimental and computational investigation on the corrosion inhibition characteristics of mild steel by some novel synthesized imines in hydrochloric acid solutions, *Corros Sci*, 92 (2015) 104.

6 Verma C, Quraishi M A, Kluza K, Makowska-Janusik M, Olasunkanmi L O & Ebenso E E, Corrosion inhibition of mild steel in 1M HCl by D-glucose derivatives of dihydropyrido [2,3-d:6,5-d′] dipyrimidine-2, 4, 6, 8(1H,3H, 5H,7H)-tetraone, *Sci Rep*, 7 (2017) 44432.

7 Sherif E M & Park S M, Inhibition of copper corrosion in 3.0% NaCl solution by N-phenyl-1,4-phenylenediamine, *J Electrochem Soc*, 152 (2005) 428.

8 Curkovic H O, Stupnisek-Lisac E & Takenouti H, The influence of pH value on the efficiency of imidazole-based corrosion inhibitors of copper, *Corros Sci*, 52 (2010) 398.

9 Pan Y C, Wen Y, Guo X Y, Song P, Shen S, Du Y P & Yang H F, 2-Amino-5-(4-pyridinyl)- 1,3,4-thiadiazole

monolayers on copper surface: Observation of the relationship between its corrosion inhibition and adsorption structure, *Corros Sci*, 73 (2013) 274.

10 Sherif E M & Park S M, 2-Amino-5-ethyl-1,3,4-thiadiazole as a corrosion inhibitor for copper in 3.0% NaCl solutions, *Corros Sci*, 48 (2006) 4065.

11 Finsgar M, Milosev I & Pihlar I, Inhibition of copper corrosion studied by electrochemical and EQCN techniques, *Acta Chim Slov*, 54 (2007) 591.

12 Amin M A, Weight loss, polarization, electrochemical impedance spectroscopy, SEM and EDX studies of the corrosion inhibition of copper in aerated NaCl solutions, *J Appl Electrochem*, 36 (2006) 215.

13 Ismail K M, Electrochemical preparation and kinetic study of poly(*o*-tolidine) in aqueous medium, *Electrochim Acta*, 52 (2007) 3883.

14 Wang C T, Chen S H, Ma H Y & Qi C S, Protection of copper corrosion by carbazole and N-vinylcarbazole self-assembled films in NaCl solution, *J Appl Electrochem*, 33 (2003) 179.

15 Sherif S M, Effects of 2-amino-5-(ethylthio)-1,3,4-thiadiazole on copper corrosion as a corrosion inhibitor in 3% NaCl solutions, *Appl Surf Sci*, 252 (2006) 8615.

16 Policarpi E B & Spinelli A, Application of Hymenaeastigonocarpa fruit shell extract as eco-friendly corrosion inhibitor for steel in sulfuric acid, *J Taiwan Inst Chem Eng*, 116 (2020) 215.

17 Bahlakeh G, Ramezanzadeh B, Dehghani A & Ramezanzadeh A, Novel cost-effective and high-performance green inhibitor based on aqueous *Peganum harmala* seed extract for mild steel corrosion in HCl solution: Detailed experimental and electronic/atomic level computational explorations, *J Mol Liq*, 283 (2019) 174.

18 Akalezi C O & Oguzie E E, Evaluation of anticorrosion properties of Chrysophyllumalbidum leaves extract for mild steel protection in acidic media, *Int J Ind Chem*, 7 (2016) 81.

19 Haldhar R, Prasad D, Nguyen L T, Kaya S, Bahadur I, Dagdag O & Kim S C, Corrosion inhibition, surface adsorption and computational studies of *Swertiachirata* extract: A sustainable and green approach, *Mater Chem Phys*, 267 (2021) 124613.

20 Chung I M, Malathy R, Priyadharshini R, Hemapriya V, Kim S H & Prabakaran M, Inhibition of mild steel corrosion using *Magnolia kobus* extract in sulphuric acid medium, *Mater Today Commun*, 25 (2020) 101687.

21 Rathod M R, Rajappa S K, Praveen B M & Bharath D K, Investigation of Dolichandra unguis-cati leaves extract as a corrosion inhibitor for mild steel in acid medium, *Curr Res Green Sustain Chem*, 4 (2021) 100113.

22 Anupama K K, Ramya K & Joseph A, Electrochemical measurements and theoretical calculations on the inhibitive interaction of *Plectranthusamboinicus* leaf extract with mild steel in hydrochloric acid, *Measurement*, 95 (2017) 297.

23 Rathod M R, Rajappa S K, Minagalavar R L, Praveen B M, Devendra B K & Kittur A A, Investigation of African mangosteen leaves extract as an environment-friendly inhibitor for low carbon steel in 0.5 M H_2SO_4, *Inorg Chem Commun*, 140 (2022) 109488.

24 Elshakre M E, Alalawy H H, Awad M I & El-Anadouli B E, On the role of the electronic states of corrosion inhibitors: Quantum chemical-electrochemical correlation study on urea derivatives, *Corros Sci*, 124 (2017) 121.

25 Tang Y, Yang X, Yang W, Chen Y & Wan R, Experimental and molecular dynamics studies on corrosion inhibition of mild steel by 2-amino-5-phenyl-1,3,4-thiadiazole, *Corros Sci*, 52 (2010) 242.

26 Moawad A, Hetta M, Zjawiony J K, Jacob M R, Hifnawy M, Marais J P & Ferreira D, Phytochemical investigation of Cycas circinalis and Cycas revoluta leaflets: Moderately active antibacterial biflavonoids, *Planta Med*, 76 (2010) 796.

27 Rathod M R & Rajappa S K, Corrosion inhibition effect of *Cycas revoluta* leaves extract on corrosion of soft-cast steel in hydrochloric acid medium, *Electrochem Sci Adv*, 2 (2021) e2100059.

28 Deora G S, Shekhawat M K & Sarswati, Ethnobotanical, phytochemical and pharmacological potential of Cycas revolute thumb: A review, *Pharmacogn J*, 12 (2020) 1165.

29 Mourya M K, Prakash A, Swami A, Singh G K & Mathur A, Leaves of cycas revoluta: Potent antimicrobial and antioxidant agent, *World J Sci Technol*, 1 (2011) 11.

30 Hsissou R, Abbout S, Seghiri R, Rehioui M, Berisha A, Erramli H, Assouag M & Elharfi A, Evaluation of corrosion inhibition performance of phosphorus polymer for carbon steel in [1 M] HCl: Computational studies (DFT, MC and MD simulations), *J Mater Res Technol*, 9 (2020) 2691.

31 Merah S, Larabi L, Benali O & Harek Y, Synergistic effect of methyl red dye and potassium iodide on inhibition of corrosion of carbon steel in 0.5 M H_2SO_4, *Pigm Resin Technol*, 37 (2008) 291.

32 Fouda A S, Ibrahim H, Rashwaan S, El-Hossiany A & Ahmed R M, Expired drug (pantoprazole sodium) as a corrosion inhibitor for high carbon steel in hydrochloric acid solution, *Int J Electrochem Sci*, 13 (2018) 6327.

33 Sasikala T, Parameswari K, Chitra S & Kiruthika A, Synthesis and corrosion inhibition study of benzodiazepines on mild steel in sulphuric acid medium, *Measurement*, 101 (2017) 175.

34 Abbar J C, Swetha G A & Sachin H P, Impact of an expired hemorheologic drug on the mitigation of zinc corrosion in acidic environment: Insights from chemical, electrochemical, and surface evaluation, *Colloids Surf A Physicochem Eng Asp*, 650 (2022) 129518.

35 Rathod M R & Rajappa S K, Corrosion protection of soft-cast steel in 1 M HCl with *Araucaria heterophylla* leaves extract, *Electrochem Sci Adv*, 2 (2021) e2100080.

36 Zheng X, Gong M, Li Q & Guo L, Investigation of 1-butyl-3-methyl-1H- benzimidazolium iodide as inhibitor for mild steel in sulfuric acid solution, *Corros Sci*, 80 (2014) 383.

37 Minagalavar R L, Rajappa S K, Rathod M R & Sajjan A M, Investigation of corrosion inhibition performance of expired fluconazole drug on mild steel in 0.5M H_2SO_4 medium, *J Mol Liq*, 391 (2023) 123291.

38 Ituen E B, Akaranta O, James A O & Shuangqin S, Green anti-corrosive oilfield chemicals from seed and leave extracts of *Griffonia simplicifolia* for mild steel, *J Chem Mater Res*, 5 (2016) 45.

39 El-Hafi M, Ezzanad A, Boulhaoua M, El-Ouasif L, Saadouni M, El-Aoufir Y, Ramli Y, Zarrouk A, Oudda H & Essassi E M, Corrosion inhibition effect of novel pyrazolo [3,4-d] pyrimidine derivative on mild steel in 1 M HCl

medium: Experimental and theoretical approach, *J Mater Environ Sci*, 9 (2018) 1234.
40 Guruprasad A, Sachin H, Swetha G & Prasanna G, Adsorption and inhibitive properties of seroquel drug for the corrosion of zinc in 0.1 M hydrochloric acid solution, *Int J Ind Chem*, 10 (2019) 17.
41 Shanmugapriya K, Prathibha B S, Vasudha V G & Nagaswarupa H P, Spathodea campanulata as a corrosion inhibitor for mild steel in 1N H_2SO_4 media, *Mater Today Proc*, 5 (2018) 22595.
42 Hebbar N, Praveen B M, Prasanna B M & Venkatesha T V, Corrosion inhibition behavior of Ketosulfone for Zinc in acidic medium, *J Fundam Appl Sci*, 7 (2015) 271.
43 Martinez S & Matikos-Hukovic M, A nonlinear kinetic model introduced for the corrosion inhibitive properties of some organic inhibitors, *J Appl Electrochem*, 33 (2003) 1137.
44 Rathod M R, Rajappa S K & Minagalavar R L, Effect of *Artabotrys odoratissimus* extract as an environmentally sustainable inhibitor for mild steel corrosion in 0.5 M H_2SO_4 media, *J Indian Chem Soc*, 99 (2022) 100445.
45 Thakur A & Kumar A, Sustainable inhibitors for corrosion mitigation in aggressive corrosive media: A comprehensive study, *J Bio Tribo Corros*, 7 (2021) 67.
46 Fouda A S, Mahmoud W M & Elawayeb K M A, Unused clopidogrel drug as eco-friendly corrosion inhibitor for carbon steel in aqueous media, *Prot Met Phys Chem*, 53 (2017) 139.
47 Luo X, Ci C, Li J, Lin K, Du S, Zhang H, Li X, Cheng Y F, Zang J & Liu Y, 4-Aminoazobenzene modified natural glucomannan as a green eco-friendly inhibitor for the mild steel in 0.5 M HCl solution, *Corros Sci*, 151 (2019) 132.
48 Preethi K P, Shetty P & Rao S A, Electrochemical measurements for the corrosion inhibition of mild steel in 1 M hydrochloric acid by using an aromatic hydrazide derivative, *Arab J Chem*, 10 (2017) 653.
49 Solomon M M, Umoren S A, Iudosoro I I & Udoh A P, Inhibitive and adsorption behaviour of carboxymethyl cellulose on mild steel corrosion in sulphuric acid solution, *Corros Sci*, 52 (2010) 1317.
50 Rathod M R, Rajappa S K & Kittur A A, Garcinia livingstonei leaves extract influenced as a mild steel efficient green corrosion inhibitor in 1 M HCl solution, *Mater Today Proc*, 54 (2022) 786.
51 Minagalavar R L, Rajappa S K, Rathod M R & Sajjan A M, Investigation of Laurus Tamala leaves extract as an environmentally acceptable corrosion inhibitor for soft steel in 1M HCl: Electrochemical, DFT, and surface characterization techniques, *Indian J Chem Technol,* 30 (2023) 492.
52 Fouda A S, El-Ewady G & Ali A H, Corrosion protection of carbon steel by using simvastatin drug in HCl medium, *J Appl Chem*, 6 (2017) 701.
53 Yasakau K, Application of AFM-based techniques in studies of corrosion and corrosion inhibition of metallic alloys, *Corros Mater Degrad,* 1 (2020) 345.
54 Minagalavar R L, Rajappa S K, Rathod M R & Sajjan A M, Experimental and theoretical investigations of cordia obliqua leaves extract as an environmentally benign inhibitor for mild steel corrosion in a 1 M HCl solution, *Port Electrochim Acta*, 42 (2024) 233.
55 Dehghani A, Bahlakeh G & Ramezanzadeh B, A detailed electrochemical/ theoretical exploration of the aqueous Chinese gooseberry fruit shell extract as a green and cheap corrosion inhibitor for mild steel in acidic solution, *J Mol Liq*, 282 (2019) 366.
56 Minagalavar R L, Rajappa S K, Rathod M R, Sajjan A M & Sujatha K, Investigation of corrosion inhibition of low carbon steel using expired drug Levocetirizine as a potential corrosion inhibitor in 0.5 M H_2SO_4 medium, *Discov Electrochem,* 2 (2025) 4.
57 Minagalavar R L, Rajappa S K, Rathod M R & Sajjan A M, Ferrous metal corrosion studies in presence of eco-friendly acacia melanoxylon leaves extract in 1M HCl condition, *Inorg Chem Commun*, 160 (2023) 111900.
58 Pai G D, Rathod M R, Rajappa S K & Kittur A A, Effect of tabebuia heterophylla plant leaves extract on corrosion protection of low carbon steel in 1M HCl medium: Electrochemical, quantum chemical and surface characterization studies, *Results Surfa Interf*, 15 (2024) 100203.
59 Minagalavar R L, Rajappa S K, Rathod M R & Sajjan A M, Corrosion mitigation of (E)-N-benzylidene-4-nitrobenzenamine on mild steel in acidic medium: Experimental and theoretical analysis, *Chem Data Collect*, 51 (2024) 101143.
60 Shashirekha, K, Aithal S, Praveen B M, Pavithra M K, Guruprasad A M, Devendra B K & Rathod M R, Experimental, electrochemical and DFT simulation studies of a novel Schiff base derivative as an efficient mild steel corrosion inhibitor in acidic environments, *Results Surf Interf*, 16 (2024) 100246.